Biofabrication DOI: 10.1088/1758-5090/aaadd3

3D Printed Lego-like Modular Microfluidic Devices Based on Capillary Driving

Jing Nie[1,2],Qing Gao[1,2], Jing-jiang Qiu[1,2], Miao Sun[3], An Liu[4], Lei Shao[1,2], Jian-zhong Fu[1,2], Peng Zhao[1,2], Yong He[1,2]*

([1]State Key Laboratory of Fluid Power and Mechatronic Systems, School of Mechanical Engineering, Zhejiang University, Hangzhou 310027, China
[2]Key Laboratory of 3D Printing Process and Equipment of Zhejiang Province, School of Mechanical Engineering, Zhejiang University, Hangzhou 310027, China
[3]Department of Oral and Maxillofacial Surgery, The Affiliated Stomatology Hospital, School of Medicine, Zhejiang University, Hangzhou, China
[4]Department of Orthopaedic Surgery, Second Affiliated Hospital of Zhejiang University School of Medicine, Hangzhou 310009, China
Corresponding to Yong He, yongqin@zju.edu.cn

Abstract

The field of how to rapidly assemble microfluidics with modular components continuously attracts researchers' attention, however extra efforts must be devoted to solving the problems of leaking and aligning between individual modules. This paper presents a novel type of modular microfluidic device, driven by capillary force. There is no necessity for a strict seal or special alignment, and its open structures make it easy to integrate various stents and reactants. The key rationale for this method is to print different functional modules with a low-cost 3D printer, then fill the channels with capillary materials and assemble them with plugs like Legos. This rapidly reconstructed modular microfluidic device consists of a variety of common functional modules and other personalized modules, each module having a unified standard interface for easy assembly. As it can be printed by a desktop 3D printed, the manufacturing process is simple and efficient, with controllable regulation of the flow channel scale. Through diverse combinations of different modules, a variety of different functions can be achieved, without duplicating the manufacturing process. A single module can also be taken out for testing and analysis. What's more, combined with basic circuit components, it can serve as a low-cost Lego-like modular microfluidic circuits. As a proof of concept, the modular microfluidic device has been successfully demonstrated and used for stent degradation and cell cultures, revealing the potential use of this method in both chemical and biological research.

Keywords：

Modular microfluidics; Capillary driving;3D printing; Liquid circuits; Lego-like microfluidics; Biofluidics

1. Introduction

Microfluidics offers a portable and automatic platform for many research fields, including analytical chemistry, biochemical analysis, biomedical research, and materials synthesis[1,2]. For example, microfluidics is an appealing choice for building a biological system in vitro [3],which can offer a convenient platform to study the mechanism of cell co-culture, cell metabolic activity, cell–cell interactions, and drug metabolism [4-7]. Recently, organ-on-a-chip technology has developed and attracted increasing interests, and some models were built to simulate the microenvironment in vivo, such as vessel-on-a–chip, and lung-on-a-chip [8, 9].However, such devices are often complicated, causing difficulty for its fabrication. What's more, monolithic microfluidic devices are not convenient for post-production modification and separately testing.

Currently, modular microfluidics assembled from individual functional modules emerged. Instead of fabricating monolithic microfluidic devices, integrated devices are assembled from a set of pre-fabricated parts. Individual modules with corresponding functions can be reconfigured and customized for new applications [10], such as biochemical analysis[11], detection of bacterial pathogens[12], chemical synthesis [13], and regenerative medicine. Each module can be designed, manufactured and modified separately before being integrated into a microfluidic system [14] and individual module can be taken out for testing after experiments. For fabricating modular microfluidics, many approaches have been reported, including microfabrication methods and 3Dprinting methods.

In the conventional microfabrication methods, Polydimethylsiloxane (PDMS) or thermoplastic materials are customized into separate modules, and assembled into a multiple functional system [11-13].Rhee and Burns developed a modular microfluidic assembly block (MAB) platform, using pre-fabricated polydimethylsiloxane (PDMS) blocks they designed Lego®-like building blocks and assembled these fluidic modules on a Lego® plate [15]. Langelier *et al*. fabricated PDMS microfluidic chips in the shape of jigsaw puzzle pieces. The interlocking tabs of the chips allowed them to interface and self-align with one another [16]. Similarly, Hsieh *et al*. demonstrated an advanced Lego®-like swappable fluidic module concept to form a fully functional microfluidic device.

Another approach is based on 3Dprinting technology. 3D printing is suggested as a new way to fabricate individual modules with the merits of automation, low cost and relatively high throughput [17, 18]. Stereolithography (SLA) was utilized by various researchers to attain a variety of microfluidic modules. In Yuen' work, motherboard, fitting components, microchannel inserts and modules with different functionalities were first fabricated via SLA, and then assembled into a SmartBuild Plug-n-Play modular microfluidic system, which is similar to the Lego concept [19]. Others employed a rather simple method. 3D printed modules were first prepared and different modular elements were finally assembled into a complete microfluidic device with the help of connectors [20].PolyJet was also taken by Lee *et al*. to create discrete building blocks and metal pins were used to connect different building blocks [21]. Meanwhile, the most common FDM technique was also applied for the construction of a water-in-oil droplet generator, sensor-integrated cell growth chamber, valve-based flow selector, and interconnectable modular devices [22].

However, there are some problems associated with the closed structure of the existing modular microfluidics. The main challenge is the accurately aligning and sealing of the system to ensure leak-free fluidic interconnections among individual modules once assembled, causing a strict demanding of the manufacturing accuracy of the modules which increases the cost. Note that it is inconvenient to load reactants on fully enclosed devices, and larger pressure is needed to drive the flow of liquid, which can bring about additional damage and leakage.

With the help of the capillary force, there is no need of enclosed flow channels or pressure to drive the flow of liquid. Microfluidic capillary systems employ surface tension effects to manipulate liquids, and are thus self-powered and self-regulated. It has been used in diagnostics in lateral flow tests [23], complex emulsion and particle generation[24, 25], drug delivery[26, 27], particle sorting[28], protein dynamics[29], and even tissue engineering[30].However, capillary systems have been limited to perform simple fluidic operations and the fabrication of glass capillary microfluidic devices is technically challenging. Recently, paper-based microfluidics has attracted renewed interest, and a lot of developments have been achieved in the field of paper-based microfluidics in analytical area and point of care systems [31-34]. So, is there any possibility that one can combine the merit of capillary driving like paper and 3D printing to fabricate both modular and pumpless microfluidics?

Here, we proposed a novel idea to design and fabricate modular microfluidic devices, driven by capillary force not by common used injection pump. A set of basic functional microfluidic modules with open channels are designed and fabricated, the channels are filled with capillary materials to drive the liquid ahead, and individual modules are assembled in a “plug-and-play” way layer by layer. Fabricated based on the low-cost 3D printer, the major modules can form a standardized series of structures and gradually make up a module library, from which the researchers can choose the corresponding modules based on the actual needs and assemble them simply. Using capillary force to achieve a continuous perfusion, this new kind pump-free microfluidic device presents open channels, which makes it convenient to deposit reactants in desired areas while avoiding the leaking and pressure problems.

2. Materials and Methods

2.1 Materials

A common desktop 3D printer (D-Force 400, Trianglelab Co., Ltd., Jiangsu, China) was used to fabricate the individual modules. A PLA filament (Alkht Co., Ltd., Beijing, China) was used as the printing material. PDMS (Sylgard 184, Dow Corning, Auburn, MI, USA) was penetrated into the surface of the modules. Then the modules were filled with Whatman No.1 filterpaper (Whatman Co., Ltd., UK), pulp mud（Colorful Handmade Paradise Co., Ltd., Liaoning, China）or a mixture of cellulose powder (Sigma-Aldrich, Shanghai, China) and deionized water (Qianjing Environmental Technology Co., Ltd., Dongguan, China). Itwas then dried in an oven (DHG-9030A, Suoyu Equipment Co., Ltd., Shanghai, China). The solution of cellulose powder and deionized water was mixed using a magnetic stirrer (84-1A, Meiyingpu Equipment Co., Ltd., Shanghai, China) to ensure the uniform distribution of the cellulose powder. Red ink, yellow ink and blue ink (Kaiguilai Co., Ltd., Shanghai, China) are used for flow channel characterization. Electrolyte solution

containing: NaCl (Macklin, Shanghai, China) and blue ink is used as liquid circuit. Tris (Macklin, Shanghai, China) and FBS containing: NaCl, $NaHCO_3$(Macklin, Shanghai, China), KCl (Macklin, Shanghai, China), $K_2HPO_4.3H_2O$ (Aladdin, Shanghai, China), $MgCl_2.6H_2O$ (Aladdin, Shanghai, China), $CaCl_2$(Aladdin, Shanghai, China), Na_2SO_4 （Macklin, Shanghai, China）, and Tris are used for degradation.

2.2 Surface modification of printed modules

The surface of the printed module is treated with a layer of PDMS to prevent sample permeation into the micro-gap of the module caused by the printing process. PDMS is prepared first by mixing the prepolymer and curing agents at a 10:1 (w/w) ratio and placed in a vacuum drying oven for degassing. Then, PDMS is poured onto the printed structure. Two minutes later, the PDMS has totally penetrated into the flaws of the module. Subsequently, the excess PDMS was wiped off, and the coated module is dried in an oven at 60 °C for 1 hour to form a sealed, thin hydrophobic layer.

2.3 Bone scaffolds biodegradation

The in vitro biodegradation of the specimens was respectively measured by placing the ceramic samples (W0, Ø25 4 mm2; n¼4) in the reaction area of the modular device, with flow channels of2mm, 4mm and 6mm in depth, as shown in Figure4-B. Then SBF and 0.05 M Tris buffer (pH 7.4) were constantly perfused using an infusion set through the flow channel at 37 °C for 2 weeks and 3 weeks, respectively, approximately corresponding with the in vivo body fluid flow rates of 1.2-6.4ml/h. The liquid supply scheme is presented in SectionS2.Control groups were statically soaked with the buffer refreshed every 48 h. After the set degradation time, the samples were gently rinsed with ethanol and dried at 80 °C to weight constancy (Wt) before being weighed with an electronic analytical balance (FA2104, Sartorius, Germany). The weight loss (degradation) is expressed as the following equation: weight loss=$(W_0-W_t)/W_0X100\%$.The biodegradation rate (i.e. solubility in vitro) of the CSi ceramics sintered at 1100–250°C was monitored by means of measuring the weight loss in two different types of buffer systems.

2.4 Cell culture

L929 mouse fibroblasts and MC3T3 cells were cultured in MEM (Tangpu Biological Technology Co., Ltd., HangZhou, China) supplemented with 10% fetal bovine serum (Tangpu Biological Technology Co., Ltd., HangZhou, China), 1% penicillin (100 units/mL), and streptomycin (100 μg/mL) (Tangpu Biological Technology Co., Ltd., HangZhou, China). RAW cells were cultured in DMEM (Tangpu Biological Technology Co., Ltd., HangZhou, China) with 10% fetal bovine serum (Tangpu Biological Technology Co., Ltd., HangZhou, China), 1% penicillin (100 units/mL) and streptomycin (100 μg/mL) (Tangpu Biological Technology Co., Ltd., HangZhou, China). All cells were incubated at 37 °C in 5% CO_2 in polystyrene tissue culture flasks. They were fed with fresh medium every other day and passaged every 4 days.

2.5 Cell-laden solution preparation

Alginate/gelatin hydrogel was used to encapsulate the cells. Sodium alginate powder (Sigma-Aldrich, Shanghai, China), gelatin powder(Sigma-Aldrich, Shanghai, China) and Calcium chloride ($CaCl_2$) powder (Sigma-Aldrich, Shanghai, China) were sterilized under UV light for half an hour, and the hydrogel solution was prepared by mixing the sodium alginate and gelatin with deionized water with a magnetic stirrer (84-1A, Meiyingpu

Equipment Co., Ltd., Shanghai, China) for 24 h at 120 rpm at 37 °C. Calcium chloride ($CaCl_2$) powder (Sigma-Aldrich, Shanghai, China) was dissolved in deionized water at 4% (w/v).

L929 mouse fibroblasts were used to prepare the cell-laden hydrogel solution. Culture flasks with 90% L929 cells confluence were washed with PBS (Tangpu Biological TechnologyCo., Ltd., Hangzhou, China) and incubated with 0.25% Trypsin-EDTA (Tangpu Biological Technology Co., Ltd., Hangzhou, China) for 3−4 min at 37 °C in 5% CO_2 to detach the cells from the culture flasks. Next, the cell suspension was centrifuged at 1,000 rpm for 5 min at room temperature, the supernatant was discarded, and the cells were resuspended in the cell culture medium to a concentration of 2×10^6 cells/ml. In this study, alginate/gelatin hydrogel was used to encapsulate the cells. The final hydrogel solution had a concentration of 2% alginate and 6% gelatin (w/v). The cell suspension was mixed with the hydrogel solution at a volume ratio of 1:1 and mixed with a magnetic stirrer for 5min at 100 rpm at 37 °C in 5% CO_2, resulting in a cell density of 1×10^6 cells/ml.

RAW and MC3T3 were used to prepare the cell suspension. Culture flasks with 90% RAW cell confluence were washed with PBS (Tangpu Biological Technology Co., Ltd., Hangzhou, China)and incubated with 0.25% Trypsin-EDTA(Tangpu Biological Technology Co., Ltd., Hangzhou, China) for 3−4 min at 37 °C in 5% CO_2 to detach the cells from the culture flasks. Next, the cell suspension was centrifuged at 1,000 rpm for 5 min at room temperature, the supernatant was discarded, and the cells were resuspended in the cell culture medium to a concentration of 4×10^4 cells/ml.

2.6 Cell biocompatibility characterization

2.6.1 Cell activity analysis

The cell viability of the samples was tested using a cell LIVE/DEAD assay. According to the instructions, first, the samples were washed with PBS three times before being stained. Next, the samples were stained using LIVE/DEAD assay reagents (Key-GEN BioTECH Co., Ltd., Nanjing, China) according to the kit instructions. Calcein AM and PI were diluted with PBS at a concentration of 2 μM and 8 μM, respectively. After incubation with the Calcein AM/PI mixture for 30−45 min in the dark, the samples were washed with PBS to remove residual reagents. Finally, a confocal fluorescence microscope (ZEISS LSM780) was used to image the cell-laden structures by acquiring two images of each frame; red and green for live and dead cells, respectively. The cell viability was calculated as the number of green stained cells/the number of total cells ×100%.

2.6.2 Cell morphology analysis

The morphology of the cells within samples was tested by cell cytoskeleton staining, including F-actin and nuclei staining. According to the kit instructions, we conducted F-actin and nuclei staining using TRITC phalloidin (Yeasen Biological Technology Co., Ltd.,Shanghai, China)and DAPI (Yeasen Biological Technology Co., Ltd. ,Shanghai, China). First, samples were washed with PBS, and fixed with 4% paraformaldehyde(Solarbio Co., Ltd., Shanghai, China) for 30 min, after which they were washed with PBS again and permeabilized with 0.5% Triton X-100 (Solarbio Co., Ltd., Shanghai, China) for 5 min. Then, the samples were washed with PBS again, and then stained with TRITC phalloidin (0.1μM) for 30 min in the dark. Next, they were washed with PBS again, and stained with DAPI (10μg/ml) for 10 min in the dark. Finally, the samples

were washed with PBS one more time and imaged using a confocal fluorescence microscope (ZEISS LSM780).

2.6.3 Cell proliferation analysis

The cell amount of the samples was tested using a cell countingKit-8（Dojindo Chemical Technology Co., Ltd., Shanghai, China）for proliferation analysis. The WST-8 in the kit can be redoxed by intracellular dehydrogenase while generating an orange-yellow formazan dye, which can be dissolved in the tissue culture medium. The amount of formazan is proportional to the number of living cells. According to the general instructions, the cell-laden samples to be tested were taken out of the device and placed in a 24-well plate. Next, the samples were washed with PBS three times. Then, 1450 μL of MEM and 50 μL of CCK-8 reagent were mixed and added to each well. Finally, after 3h of incubation, the solution was transferred to a 96-well plate, with 200 μL for each well in 5 parallel groups. The optical density at a wavelength of 450 nm was measured with a microplate reader.

2.7 cytotoxicity testing

The cell amount in the transwell plates was tested using a cell countingKit-8 (Dojindo Chemical Technology Co., Ltd., Shanghai, China)for cytotoxicity analysis. The WST-8 in the kit can be redoxed by intracellular dehydrogenase while generating an orange-yellow formazan dye, which can be dissolved into the tissue culture medium. The amount of formazan is proportional to the number of living cells. According to the general instructions, L929 cells wereseeded in 24-well transwell plates at a density of 5×10^4 cells/well and incubated for 24 hours for cell adherence. Next, the materials to be tested were added to each well and cultured for 1, 2, 3 days. The control group was incubated without adding any additional materials. Then, the culture medium was removed and samples were washed with PBS three times, after which 1450 μL of MEM and 50 μL of CCK-8 reagent were mixed and added to each well. Finally, after 3h of incubation, the solution was transferred to a 96-well plate, with 200μLfor each well in 5 parallel groups. The optical density at a wavelength of 450 nm was measured with a microplate reader.

3. Results and Discussion

3.1 Fabrication process

The key point of this method is to fabricate different functional PLA modules and to assemble them quickly with plugs like Legos. The fabrication process for the modular microfluidic device in this study is shown in Figure 1. Several steps are involved in constructing a modular microfluidic device.

Before printing, each module pattern is designed with computer aided design (CAD) software. First, individual modules are printed. Next, a thin layer of polydimethylsiloxane (PDMS) is penetrated into the surface of the module to seal the micro gap generated during the 3D printing process. Then, according to the specific needs, certain modules from the module library are assembled layer by layer. Finally, pulp mud is smeared into the channels, and it can be used after drying naturally. The detailed comparison between different capillary materials is provided in section S1 in the Supporting Information, and the whole manufacturing process are displayed in Video S1.

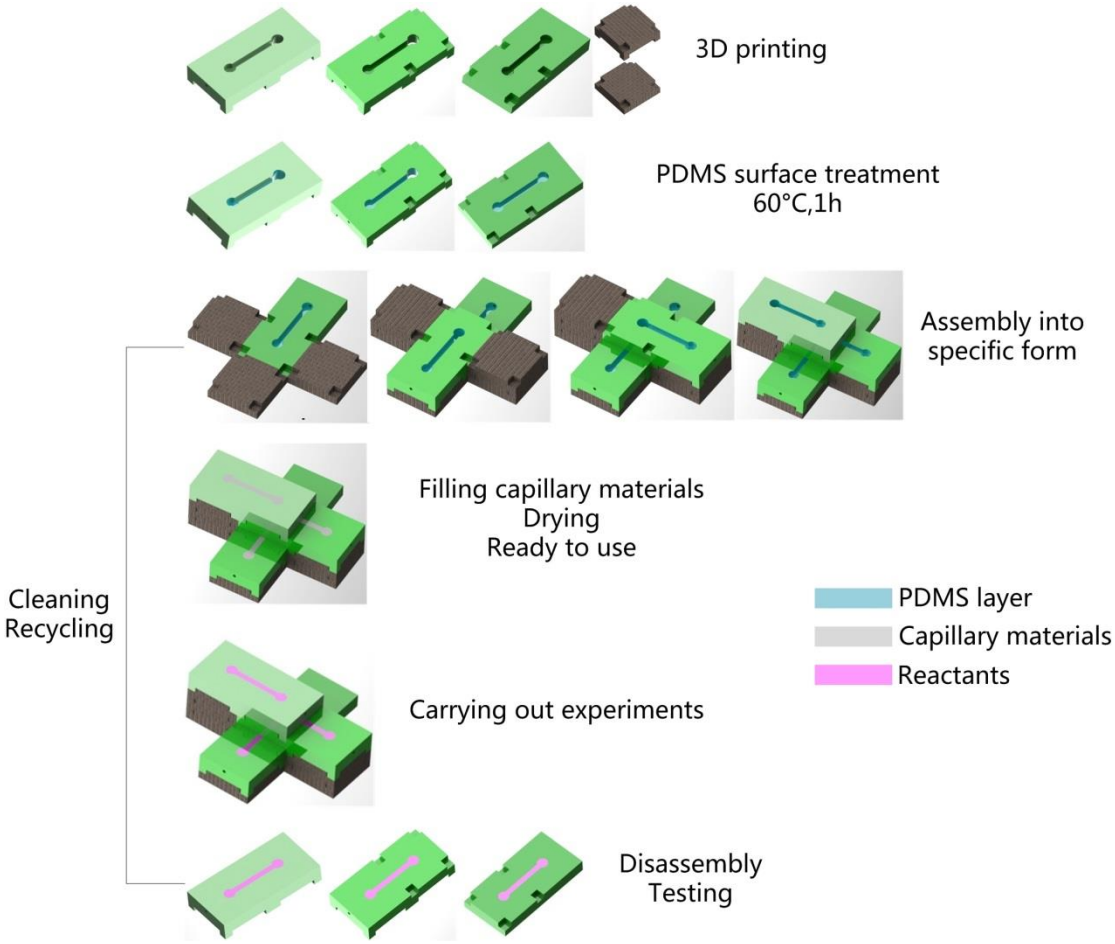

Figure 1. Schematic of fabrication process for the modular microfluidic device: Individual modules are printed, and then PDMS is used to treat the surface. Complete microfluidic system is formed after assembly of specific modules and filling of capillary materials into the flow channels of each module. After the experiment, the system is disassembled and particular modules can be taken out for testing. Finally, all the modules can be recycled after cleaning.

3.1.1 Design of units

As shown in Figure 2-A, the individual unit compromises several components：male plug, female plug, inlet, connection hole, flow channel, and reaction area. The common modules have a uniform interface including a male plug and a female plug, and they are matched in size for assembly. The design of the reaction zone is adapted to specific reactants and experiment conditions. The flow channels are designed according to the requirements of the flow rates, and the theoretical basis of the speed programming is introduced in Section S3. The inlet is matched with the liquid supply of the infusion set. As for the size of individual modules, there is a smallest unit size, and the modules sizes are integer expansions of the smallest unit for uniformity. These parameters can also be designed individually according to specific needs.

According to the design principles, several different basic modules and other personal functional modules are designed. There are several basic modules：valve module (utilizing the structure of ball-point pen to control the flowing), connection module (to achieve the connecting of the flow channels), flow channel module (presenting flow channels of different sizes to achieve speed programming), cover module (covering the

specific area to prevent contamination and interference), support module (playing a supporting role), mixing module (design of the serpentine runner to make the reactants thoroughly mixed), concentration module (distribution of the flow channels in the form of a Christmas tree for the formation of the concentration gradient), culture module (including a reaction area for reactants loading to proceed reaction), collection module (for product collection) and so on, as shown in Figure 2 B-H. Video S2 shows the detailed characteristics of every basic module.

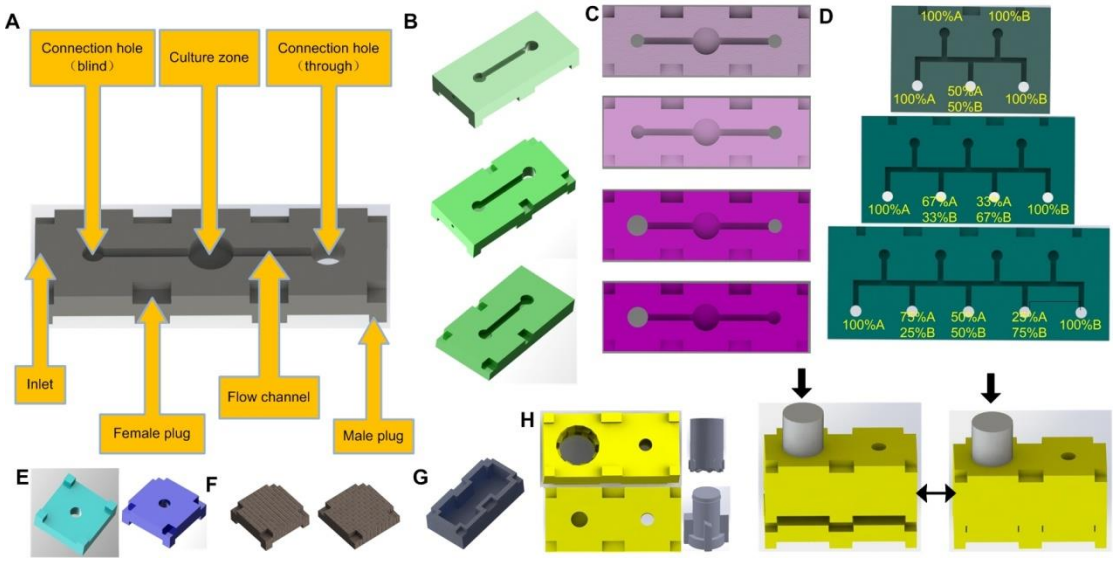

Figure 2.Schematic of several basic functional modules used for assembly of a complete microfluidic device. A. General components of individual modules. B. Several forms of flow channel modules. C. Several forms of culture modules. D. Several forms of concentration modules. E. Several forms of connection modules. F. Several forms of support modules. G. Collection module. H. Valve module: components, off-state, on-state.

3.1.2 Fabrication of unit

Before printing, each module pattern is designed with a computer aided design (CAD) software. The pattern CADs are then exported as STL files and converted into G code with 3D printing software. The fused PLA ink is directly printed following the designed path which is controlled by G code. The printing time for each module depends on the size of the module, and most of them can be finished in just 10 minutes. After that, the surface of the module is modified with a layer of PDMS.

3.1.3 Assembly into a complete microfluidic system

Based on the manufacturing process above, a few modules are prepared to form different functional microfluidic systems according to the design of the integrated system.

A complete microfluidic device is created by stacking a set of modules together by its male and female plugs. Every individual module has female plugs on the top surface, and male plugs on the bottom surface. The female plugs and the male plugs are matched in size, so that two modules can be aligned and installed together.

The minimal time from the fabrication of the individual modules to the final assembly of a microfluidic system is approximately 30 minutes. Thus, rapid construction of an integrated microfluidic system can be achieved with low cost and high throughput. The various assembly forms and equivalent schematics are shown in Figure3-D, and the

assembly process of these models are shown in Video S2.

3.1.4 Liquid loading and modular microfluidic circuits

Take the four-story structure and multistage co-culture model for example，we conducted the mixing of inks of different colors to watch the color changes. As shown in Figure3 A-B, the mixing of the three inks and the formation of the concentration gradient were realized. Video S1 shows the timing loading and mixing process of three inks. Section S4 fully demonstrated the results of the mixing experiment.

Using the electrolyte solution as a conductive carrier, we also conducted traffic light simulation and timing lighting experiments on the modular microfluidic system, as shown in Figure 3-C.In Section S5, the factors influencing the resistance of liquid circuit are analyzed qualitatively. VideoS1 shows that conduction order depends on the arrangement of electronic components, and conduction time depends on the arrival of the electrolyte solution, which is related to the flow rate and flow channel length. The traffic light simulation effect is shown in Video S1, and the source code of the traffic light simulation is presented in Section S6.

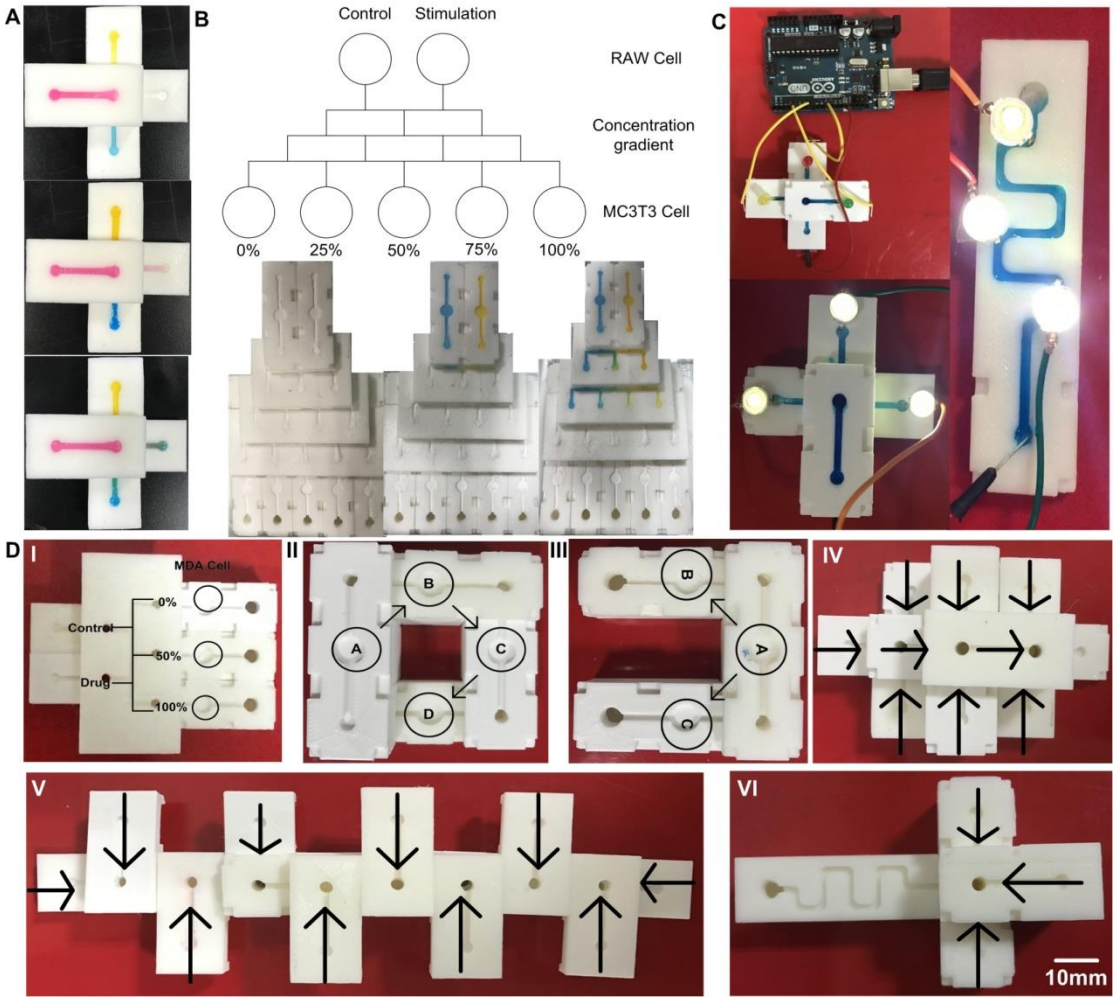

Figure 3.Schematic of several different forms of the modular microfluidic device. A. B. Flowing and mixing experiments of several forms. C. Circuit display of the device. D. Extended assembly forms and equivalent schematics: multistage coculture, cascade effect, drug screening, parallel control, and timing mixing.

3.2 Bone scaffold degradation

In order to prove the dynamic perfusion merit of the device as a bioreactor, degradation of bone scaffolds was carried out using this device. Section S2 shows how the equipment works. The results are compared with degradation of the static soaking condition.

As can be seen from Figure 4-A& Figure 4-C, on the constant perfusion condition, the biodegradation rate was much higher than that of the static soaking condition. Also，flow channels with a depth of 2,4,6 mm were tested. The results show that the biodegradation rate increased with the flow channel depth in both of the buffer systems.

Other stents can also be integrated in the modular system for corresponding research, such as micro-nano composite scaffold, electrospinning PCL film,polystyrene wafer, silicone film, filter paper and hydrogel structures, as shown in Figure 4-D.

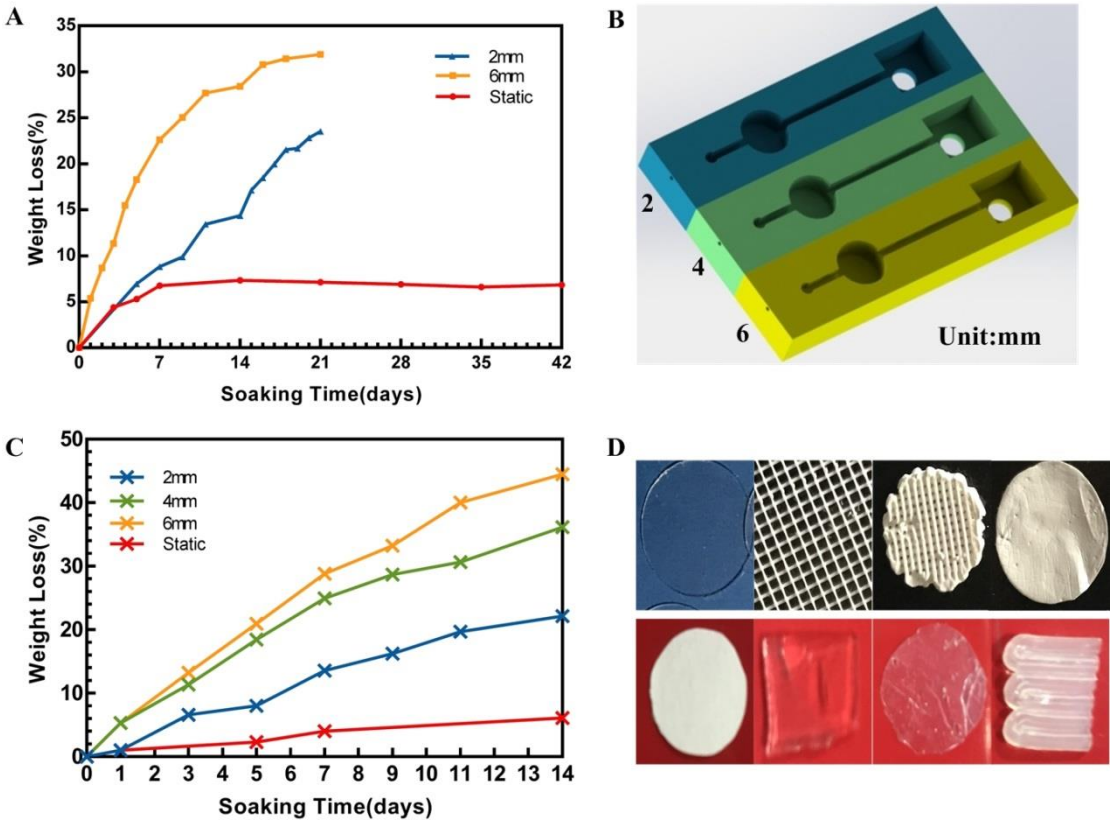

Figure 4.Degradation testing of CSi ceramic scaffolds on the dynamic perfusion and static soaking conditions. A. The weight loss of the ceramic scaffolds in the SBF condition. B. The weight loss of the ceramic scaffolds in the Tris condition. C. Reaction devices for dynamic perfusion. D. Various kinds of scaffolds that can be integrated in the system.

3.3 Cell culture

To evaluate the biocompatibility of the fabrication method, we conducted 3D culture of L929 mouse fibroblasts on perfusion condition using the device. Also, in order to demonstrate the potential capability for the cell-cell interaction of the device, we carried out a 2D culture of the RAW and MC3T3 on perfusion condition. Section S2 shows how the equipment works.

3.3.1 3D culture of L929 on perfusion condition

We mixed L929 mouse fibroblasts with alginate-gelatin solution to cast cell-laden

hydrogel wafer structures. Then, the cell-laden wafers, which were 1mm thick and 6 mm in diameter, were placed in the culture areas of the culture modules within the system. Perfusion with MEM at a flow rate of approximately 1mL/h using the liquid supply of the infusion set, they were cultured at 37 °C in 5% CO_2.

The cell viability of the wafer structures was tested after 1, 4, 7 and 10 days of the culture using a cell LIVE/DEAD assay. In this experiment, 12 samples with 1mm depth and 6 mm diameter were cast, and three samples were concurrently used in a cell viability analysis on day 1, day 4, day 7, and day 10. For the dynamic culture, the live/dead assay showed that almost all cells remained alive and were stained green. A small amount of dead cells, stained red, were observed. For 10 days of the in vitro culture, cells within the wafer structures on the modular device showed spherical proliferation, while maintaining high viability of more than 90%, as shown in Figure5-A.

The morphology of the cells within the wafer structures was tested after 1, 4, 7 and 10 days of the culture by cell cytoskeleton staining, including F-actin and nuclei staining. For the dynamic culture, the cell cytoskeleton staining showed that cells wrapped in hydrogels have a spherical proliferation trend with the spherical size becoming gradually larger, as shown in Figure5-B.

The cell amount of the wafer structures was tested after 1, 4, 7 and 10 days of the culture using a cell countingKit-8（CCK-8）for proliferation analysis. The results show that the proliferation rate of the dynamic group was higher than that of the static group after 10 days of the culture, as shown in Figure5-C.

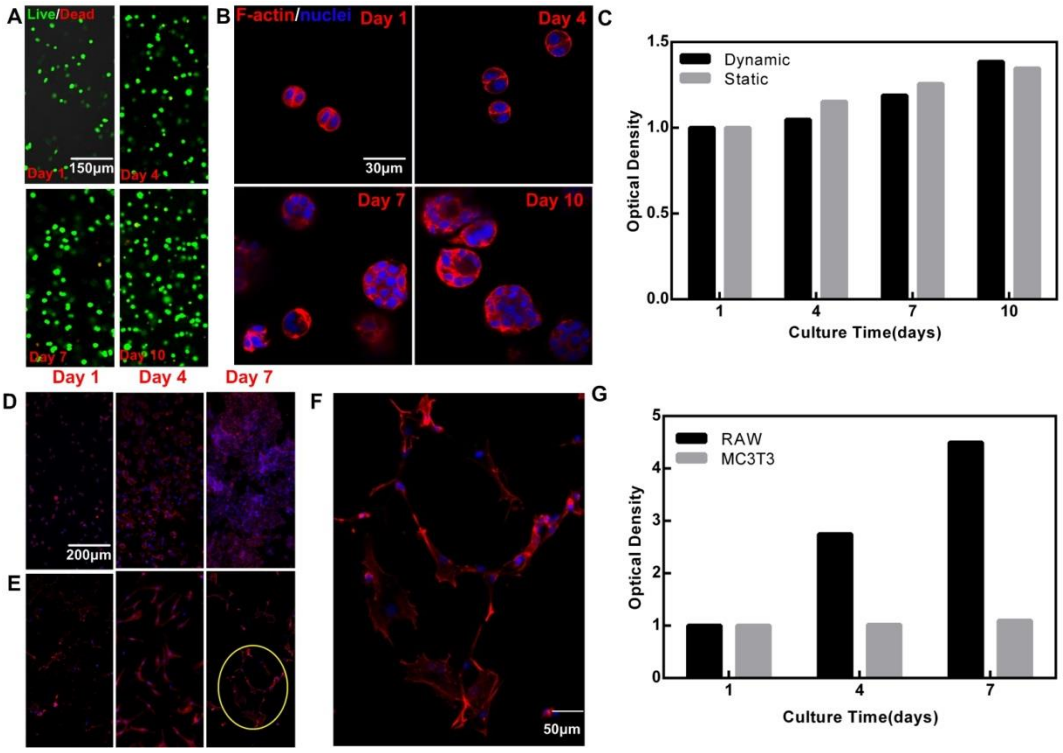

Figure 5.3D dynamic culture of L929 cells and 2D dynamic culture of RAW cells and MC3T3 cells. A. Cell cytoskeleton staining after 1, 4, 7, 10 days. B. Cell viability staining after 1, 4, 7, 10 days. Calcein-AM (green) for live cell and PI (red) for dead cell were used to measure the cell viability. C. Quantitative analysis of cell proliferation rate after 1, 4, 7, 10 days in comparison with static condition. D. Cell cytoskeleton staining of RAW cells after 1, 4, 7, days. E. Cell cytoskeleton staining of MC3T3 cells after 1,

4, 7, days. F. Partial magnification of the yellow circle zoom. G. Quantitative analysis of cell proliferation rate after 1, 4, 7 days for two kinds of cells.

3.3.2 2D culture of RAW and MC3T3 on perfusion condition

RAW and MC3T3 were seeded on polystyrene wafers with a cell density of 4×10^4 cells/wafer. The wafers were 6mm in diameter and 1mm thick. When the cell-laden polystyrene wafers were placed in the cell culture zones of the fabricated microfluidic devices, the cells were cultured at 37 °C in 5 % of CO_2, perfusion with MEM at a flow rate of approximately 1mL/h using the liquid supply of the infusion set.

The cell morphology of the wafer structures was tested after 1, 4and 7 days of culture using cell cytoskeleton staining, including F-actin and nuclei staining. The results show that the RAW cells appeared to be in a soaring state, while the MC3T3 cells gradually established contact with each other, as shown in Figure5D-F.

The cell amount of the wafer structures was tested after 1, 4and 7 days of the culture using a cell countingKit-8（CCK-8）for proliferation analysis. The results show that the proliferation rate of the RAW cells was significantly higher than that of the MC3T3 cells, as shown in Figure5-G.

4. Conclusions

In this study, a modular microfluidic system based on capillary driving is proposed. Consisting of a series of different modules, it can be combined into various forms with diverse functions for different applications. The system exhibits improved flow rate programmability and good biocompatibility, suggesting significant potential applications in bioreactors.

We have developed a method to establish a modular microfluidic system by simply assembling individual basic modules together according to the specific needs of the experiment. We have proposed a series of functional modules and assembly forms. We have determined an ideal material for the filling of the flow channels after a multifaceted comparison of several capillary materials. We also studied the elements that influence the flow rate of the flow channel. In addition, we carried out a series of experiments on the system to prove its functionality and diversity. As a proof of concept, the modular microfluidic device has been successfully demonstrated and used for stent degradation and cell culture, revealing the potential use of this device in chemical and biological research.

Supporting Information

The Supporting Information is available free of charge on the website at DOI:

Flow channel filling material; liquid supply and encapsulation; speed programming; color experiment results; modular liquid circuit resistance; and source code of the traffic light simulation (PDF)

Manufacturing process of a modular microfluidic device and function display (Video S1); individual modules display and assembly process of several functional forms (Video S2)

Acknowledgements

This paper was sponsored by the National Nature Science Foundation of China (No. 51622510, U1609207), the Science Fund for Creative Research Groups of the National Natural Science Foundation of China (no. 51521064), the Nature Science Foundation of Zhejiang Province, China (No. LR17E050001) ,the Fundamental Research Funds for the Central Universities. The helpful discussions from Dr. Xiao Li, Stanford University is appreciated.

Reference

1. Whitesides G M. The origins and the future of microfluidics[J]. Nature, 2006, 442(7101): 368-373.
2. Weibel D B, Whitesides G M. Applications of microfluidics in chemical biology[J]. Current opinion in chemical biology, 2006, 10(6): 584-591.
3. Sackmann E K, Fulton A L, Beebe D J. The present and future role of microfluidics in biomedical research[J]. Nature, 2014, 507(7491): 181-189.
4. Esch M B, Prot J M, Wang Y I, et al. Multi-cellular 3D human primary liver cell culture elevates metabolic activity under fluidic flow[J]. Lab on a Chip, 2015, 15(10): 2269-2277.
5. Chen M B, Srigunapalan S, Wheeler A R, et al. A 3D microfluidic platform incorporating methacrylated gelatin hydrogels to study physiological cardiovascular cell–cell interactions[J]. Lab on a Chip, 2013, 13(13): 2591-2598.
6. Gao D, Liu H, Lin J M, et al. Characterization of drug permeability in Caco-2 monolayers by mass spectrometry on a membrane-based microfluidic device[J]. Lab on a chip, 2013, 13(5): 978-985.
7. Jang K J, Suh K Y. A multi-layer microfluidic device for efficient culture and analysis of renal tubular cells[J]. Lab on a chip, 2010, 10(1): 36-42.
8. Huh D, Leslie D C, Matthews B D, et al. A human disease model of drug toxicity–induced pulmonary edema in a lung-on-a-chip microdevice[J]. Science translational medicine, 2012, 4(159): 159ra147-159ra147.
9. Wang X, Phan D T T, Sobrino A, et al. Engineering anastomosis between living capillary networks and endothelial cell-lined microfluidic channels[J]. Lab on a Chip, 2016, 16(2): 282-290.
10. Vittayarukskul K, Lee A P. A truly Lego®-like modular microfluidics platform[J]. Journal of Micromechanics and Microengineering, 2017, 27(3): 035004.
11. Shaikh K A, Ryu K S, Goluch E D, et al. A modular microfluidic architecture for integrated biochemical analysis[J]. Proceedings of the National Academy of Sciences of the United States of America, 2005, 102(28): 9745-9750.
12. Chen Y W, Wang H, Hupert M, et al. Modular microfluidic system fabricated in thermoplastics for the strain-specific detection of bacterial pathogens[J]. Lab on a Chip, 2012, 12(18): 338-3355.
13. Li W, Greener J, Voicu D, et al. Multiple modular microfluidic (M 3) reactors for the synthesis of polymer particles[J]. Lab on a Chip, 2009, 9(18): 2715-2721.
14. Hsieh Y F, Yang A S, Chen J W, et al. A Lego®-like swappable fluidic module for bio-chemapplications[J]. Sensors and Actuators B: Chemical, 2014, 204: 489-496.
15. Rhee M, Burns M A. Microfluidic assembly blocks[J]. Lab on a Chip, 2008, 8(8): 1365-1373.
16. Langelier S M, Livak-Dahl E, Manzo A J, et al. Flexible casting of modular self-aligning microfluidic assembly blocks[J]. Lab on a Chip, 2011, 11(9): 1679-1687.
17. Bhattacharjee N, Urrios A, Kang S, et al. The upcoming 3D-printing revolution in microfluidics[J]. Lab on a Chip, 2016, 16(10): 1720-1742.
18. Waheed S, Cabot J M, Macdonald N P, et al. 3D printed microfluidic devices: enablers and barriers[J]. Lab on a Chip, 2016, 16(11): 1993-2013.
19. Yuen P K. SmartBuild–A truly plug-n-play modular microfluidic system[J]. Lab on a Chip, 2008, 8(8): 1374-1378.
20. Bhargava K C, Thompson B, Malmstadt N. Discrete elements for 3D microfluidics[J]. Proceedings of the National Academy of Sciences, 2014, 111(42): 15013-15018.
21. Lee K G, Park K J, Seok S, et al. 3D printed modules for integrated microfluidic devices[J]. RSC Advances, 2014, 4(62): 32876-32880.

22. Tsuda S, Jaffery H, Doran D, et al. Customizable 3D printed 'plug and play'millifluidic devices for programmable fluidics[J]. PLoS One, 2015, 10(11): e0141640.

23. Haeberle S, Zengerle R. Microfluidic platforms for lab-on-a-chip applications[J]. Lab on a Chip, 2007, 7(9): 1094-1110.

24. Utada A S, Lorenceau E L, Link D R, et al. Monodisperse double emulsions generated from a microcapillary device[J]. Science, 2005, 308(5721): 537-541.

25. Duncanson W J, Lin T, Abate A R, et al. Microfluidic synthesis of advanced microparticles for encapsulation and controlled release[J]. Lab on a Chip, 2012, 12(12): 2135-2145.

26. Benson B R, Stone H A, Prud'homme R K. An "off-the-shelf" capillary microfluidic device that enables tuning of the droplet breakup regime at constant flow rates[J]. Lab on a chip, 2013, 13(23): 4507-4511.

27. Windbergs M, Zhao Y, Heyman J, et al. Biodegradable core–shell carriers for simultaneous encapsulation of synergistic actives[J]. J. Am. Chem. Soc, 2013, 135(21): 7933-7937.

28. Terray A, Hart S J. "Off-the-shelf" 3-D microfluidic nozzle[J]. Lab on a Chip, 2010, 10(13): 1729-1731.

29. Burke K S, Parul D, Reddish M J, et al. A simple three-dimensional-focusing, continuous-flow mixer for the study of fast protein dynamics[J]. Lab on a Chip, 2013, 13(15): 2912-2921.

30. Onoe H, Okitsu T, Itou A, et al. Metre-long cell-laden microfibres exhibit tissue morphologies and functions[J]. Nature materials, 2013, 12(6): 584.

31. Cate D M, Adkins J A, Mettakoonpitak J, et al. Recent developments in paper-based microfluidic devices[J]. Analytical chemistry, 2014, 87(1): 19-41.

32. He Y, Wu Y, Fu J Z, et al. Fabrication of paper-based microfluidic analysis devices: a review[J]. RSC Advances, 2015, 5(95): 78109-78127.

33. Martinez A W, Phillips S T, Butte M J, et al. Patterned paper as a platform for inexpensive, low‐volume, portable bioassays[J]. AngewandteChemie International Edition, 2007, 46(8): 1318-1320.

34. He Y, Gao Q, Wu W B, et al. 3D Printed Paper-Based Microfluidic Analytical Devices[J]. Micromachines, 2016, 7(7): 108.

Biofabrication DOI: 10.1088/1758-5090/aaadd3

3D Printed Lego-like Modular Microfluidic Devices Based on Capillary Driving

Jing Nie[1,2],Qing Gao[1,2], Jing-jiang Qiu[1,2], Miao Sun[3], An Liu[4], Lei Shao[1,2], Jian-zhong Fu[1,2], Yong He[1,2]*

([1]State Key Laboratory of Fluid Power and Mechatronic Systems, School of Mechanical Engineering, Zhejiang University, Hangzhou 310027, China
[2]Key Laboratory of 3D Printing Process and Equipment of Zhejiang Province, School of Mechanical Engineering, Zhejiang University, Hangzhou 310027, China
[3]Department of Oral and Maxillofacial Surgery, The Affiliated Stomatology Hospital, School of Medicine, Zhejiang University, Hangzhou, China
[4]Department of Orthopaedic Surgery, Second Affiliated Hospital of Zhejiang University School of Medicine, Hangzhou 310009, China
Corresponding to Yong He, yongqin@zju.edu.cn

1 Flow channel filling material

The capillary force is the driving force, so the microstructure of the pulp mud, cellulose powder and filter paper are investigated by comparison, as shown in Figure S1a-f. Compared to the filter paper, the surface morphology of the cellulose powder is more ordered, which is beneficial for keeping a steady flow and a uniformity of the microscale solution dispersion. Compared to the filter paper and cellulose powder, the pulp mud has a controllable and stable thickness, which enables the 3D filling of the materials into the channels.

In terms of vibration or instability, the pulp mud channels prevent damage. For a large flow rate case, the pulp mud channels are not washed away. The pulp mud has a muddy or cream form, which makes it easy to fill the pulp mud into the various channels. Also, its muddy form allows the pulp mud to be stuffed into the channels, which can improve the channel resolution. For multi-layer assembly, the leakage between different layers will appear in the course of the liquid filling, which will cause filling failure. Fortunately, the muddy form of the pulp mud will greatly address this problem. Also, natural drying decreases the material shrinkage, because of the intense drying process.

We use the cell countingKit-8（CCK-8）for cytotoxicity testing. According to the general instructions, the filling materials to be tested were added to each well and cultured for 1, 2, 3 days. The control group was incubated without adding any additional materials.

The result shows that compared with the blank group, the three materials all have a certain toxicity, which does not obviously affect cell proliferation. As shown in Figure S1-g, among them, the filter paper has the minimal toxicity, while the toxicity of the pulp mud is slightly higher than that of the filter paper, and the cellulose powder has the highest toxicity.

In summary, the pulp mud is an ideal material for the fabrication of 3D microfluidic devices.

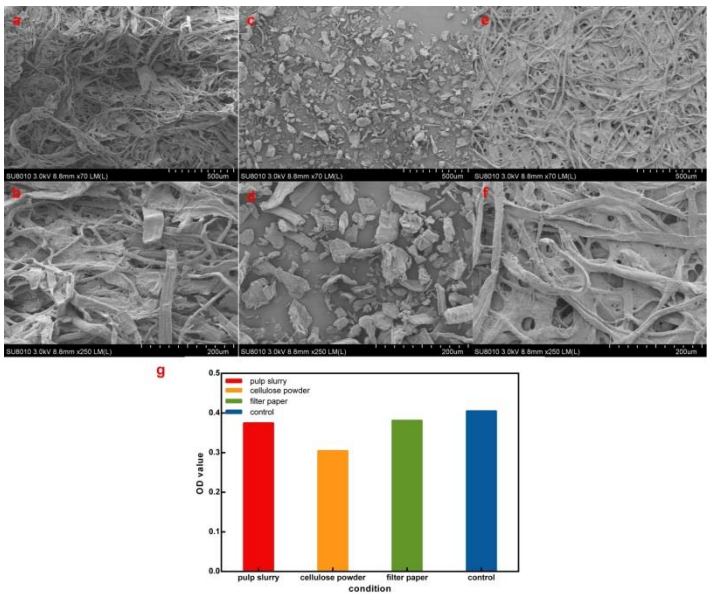

Figure S1. Characteristics of the filling materials. a-f. Scanning electron microscopy of the filling materials. a. Microstructure of pulp mud under microscope (70×). b. Microstructure of pulp mud under microscope (250×). c. Microstructure of cellulose powder under microscope (70×). d. Microstructure of cellulose powder under microscope (250×). e. Microstructure of filter paper under microscope (70×). f. Microstructure of filter paper under microscope (250×).g. Cell toxicity testing of the filling materials.

2 Liquid supply and encapsulation

Driven by the capillary force，the system does not require an extra pump to supply the driving force, it only needs a liquid supply . A gravity-based infusion set is an ideal choice, as shown in Figure S2-a. Without needing external power, it is cost-effective, convenient and portable. Also, the needles match the inlet holes. The liquid supply speed is regulated by the distance between the liquid level and the needle, as shown in Figure S2-d.

As an open channel microfluidic analytical device, unprotected channels are potential sources of sample contamination, particularly when directly exposed to the air. As the individual modules are fabricated by a D3DP, it is very easy to print a cover module as a protecting mask. For real-time observation, transparent Acrylic and Polystyrene plate lids are good choices for covering. Figure S2 a-c shows how the equipment works.

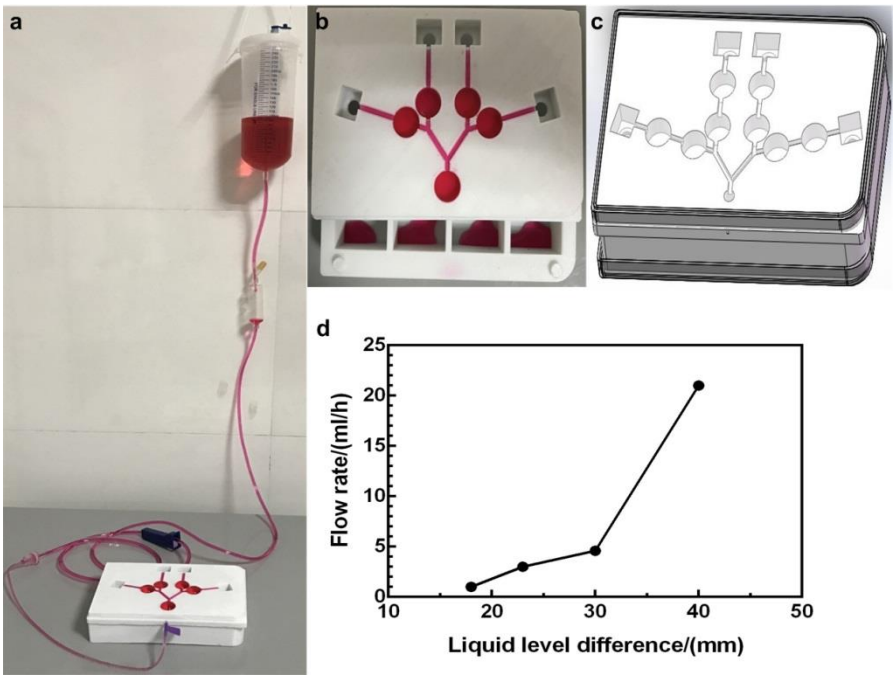

Figure S2. Schematic of how the equipment works. a. The liquid supply scheme. b. Product collection scheme. c. Encapsulation and capping scheme. d. The relationship between the flow rate and the liquid level difference.

3 Speed programming

With the help of 3D printing, it is easy to print a 3D channel with any shape parameters. Therefore, regulating the flow rates by adjusting the channel geometric shapes becomes possible. Several factors, namely channel width, channel depth and bifurcation angle, influence the flow rate of the liquid in a channel. Here, we describe research conducted to examine the relationship among channel width, channel depth, bifurcation angle and flow rate under the condition of capillary driving.

After further studying the effect on the flow rate of flow channel length, width, depth and bifurcation angle, it was found that the channel width is proportional to the flow rate, the flow channel depth and flow rate are inversely proportional to each other, and different branch angles have some influence on the flow rate. Interestingly, similar to the vein structure of a leaf, the angle of 75 degrees for the two branches is found to be most conducive to the flow of liquid, as shown in Figure S3-k. As a result, through the design of different depths, widths and distribution angles for the flow channels, controllably regulating the flow rate can be easily achieved. Different shapes, sizes, and location distribution of the flow channels can be easily achieved with the 3D printer, and we can further control the flow rate within the flow channels.

When the red dye is delivered into the center of a capillary microfluidic chip, the flow trend corresponding with the width of the channels can be found, as shown in Figure S3 c-d. The flow trend corresponding with the depth of the channels is shown in Figure S3-g, and the flow trend corresponding with the bifurcation angles is shown in Figure S3-j.

Additionally, special devices are fabricated to investigate the quantitative relationships between channel depth, channel width, bifurcation angle and flow rate.

The six channels on the device are all 2 mm deep and 30 mm long and have a width

gradient from 1 to 6 mm, as shown in Figure S3-b. The red dye was injected using a syringe pump with a flow rate of 1 mL/h through the inlet of each channel. A line chart of the relationship between channel width and flow time is shown in Figure S3-a. The flow time exhibits a linear relationship with the channel width. Thus, it is very easy and convenient to control the flow rate by regulating the channel width.

The eight channels on the device are all 2 mm wide and 30 mm long and have a depth gradient of 0.5 to 4 mm, as shown in Figure S3-f. The red dye was injected using a syringe pump with a flow rate of 1 mL/h through the inlet of each channel. A line chart of the relationship between channel depth and flow time is shown in Figure S3-e. The flow time exhibits a linear relationship with the channel depth. Thus, it is very easy and convenient to control the flow rate by regulating the channel depth.

The six channels on the device are all 2 mm wide, 2mm deep and 30 mm long with a bifurcation in the same area and have a bifurcation angle gradient of 15 to 90 °, as shown in Figure S3-i. The red dye was injected using a syringe pump with a flow rate of 1 mL/h through the inlet of each channel. A line chart of the relationship between bifurcation angle and flow time is shown in Figure S3-h. Thus, it is very easy and convenient to control the flow rate by regulating the channel depth after quantitative calibration.

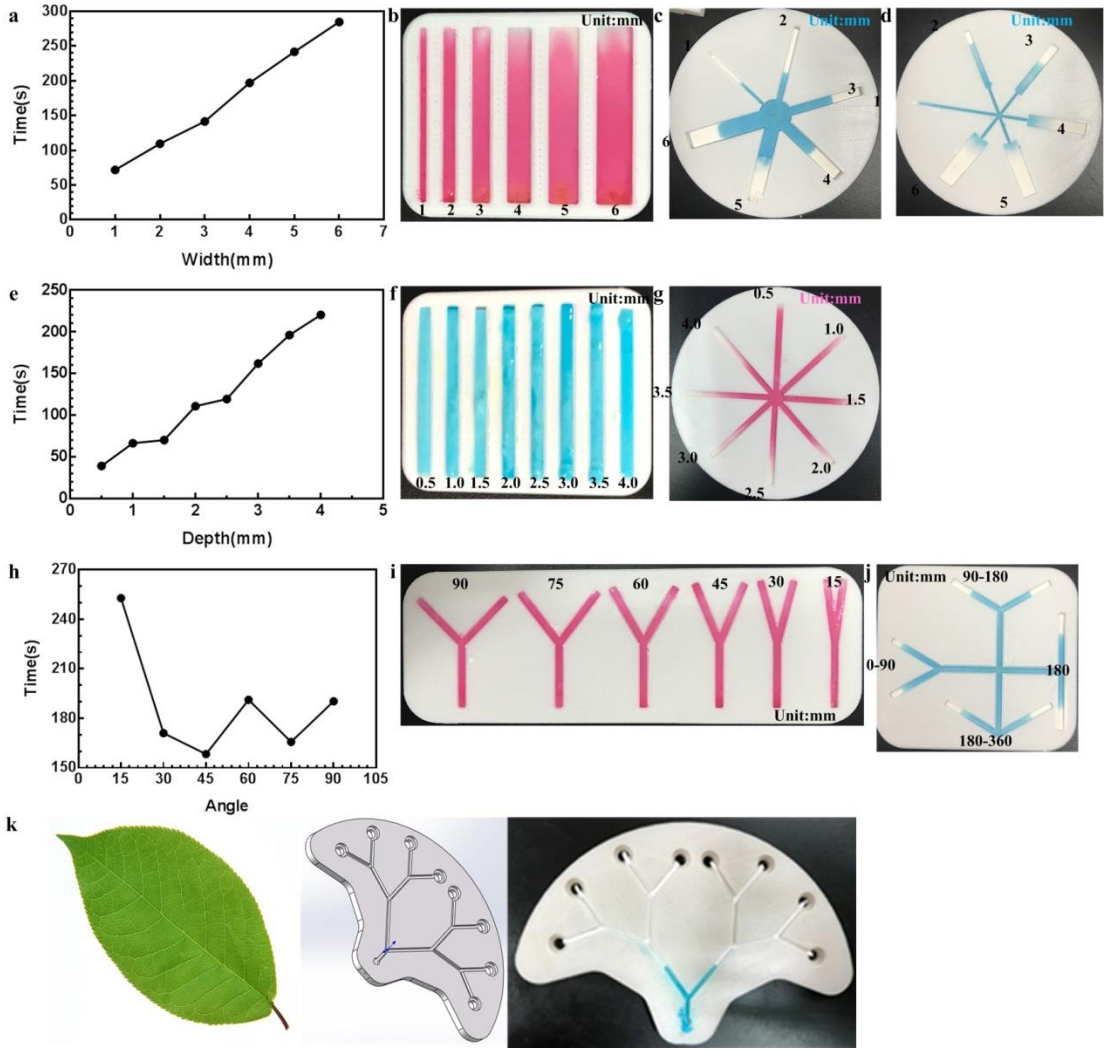

Figure S3. Relationship between channel shape and flow time and schematic of the entire microfluidic

device. a, b. Quantitative analysis of the relationship between channel width and flow time. c, d. The flow trend of blue dye in 6 channels with a gradient width. e, f. Quantitative analysis of the relationship between channel depth and flow time. g. The flow trend of red dye in 8 channels with a gradient depth. h, i. Quantitative analysis of the relationship between channel bifurcation angle and flow time. j. The flow trend of blue dye in 4 channels with a gradient bifurcation angle. k. Design of bionic veins for the channel bifurcation angle.

4 Color experiment results

Take the four-story structure and multistage co-culture model for example，we conducted the mixing of inks of different colors to watch the color changes. The experimental results show that the mixing of the three inks and the formation of the concentration gradient were realized and the final mixing color are in accordance with the direct mixing results of the three inks, as shown in the Figure S4 a-c. After the experiment, the whole system is split into single modules, which can be used for characterization and subsequent detection. The front and back pictures of the modules show that there are not leakage problems in the system, as shown in the Figure S4 d-f.

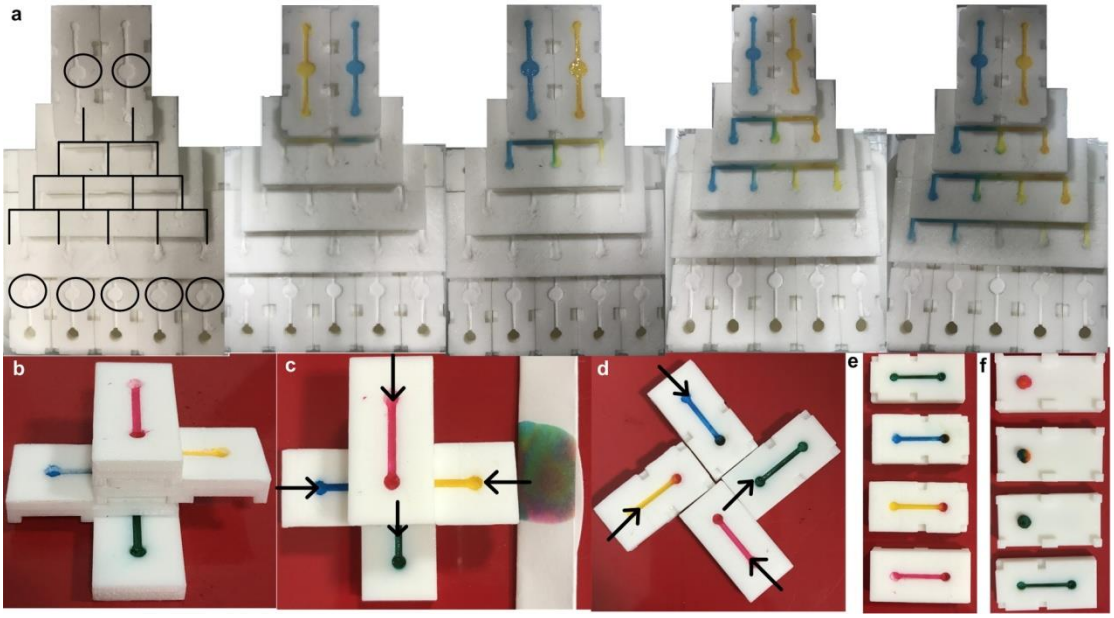

Figure S4. Experimental results of ink loading. a. Experimental results of formation of concentration gradient. b. Experimental results of mixing of inks of three colors. c. Comparison with direct mixing of three inks. d. e. f. Modules disassembled from the whole system.

5 Modular liquid circuit resistance

As shown in Figure S5, with the length increasing, the width decreasing, the brightness of the light becomes darker.

brightness$\propto\frac{1}{R}$

R=$\rho\frac{l}{S}$, resistivity (ρ), flow channel length (l), cross-sectional area (S)

$\rho\propto\frac{1}{n}$, electrolyte solution concentration (n)

S=w*t , flow channel width (w), filter paper thickness (t)

Liquid volume$\propto$l*S

Figure S5. Modular liquid circuit resistance. a. b. Comparison between different flow channel widths. c. Comparison between different flow channel lengths.

6 The source code of the traffic light simulation

```
intredled =10;
intyellowled =7;
intgreenled =4;
void setup()
{
pinMode(redled, OUTPUT);
pinMode(yellowled, OUTPUT);
pinMode(greenled, OUTPUT);
}
void loop()
{
digitalWrite(redled, HIGH);
delay(1000);
digitalWrite(redled, LOW);
digitalWrite(yellowled, HIGH);
delay(200);
digitalWrite(yellowled, LOW);
digitalWrite(greenled, HIGH);
delay(1000);
digitalWrite(greenled, LOW);
}
```